Theory of thermionic emission from a two-dimensional conductor and its application to a graphene-semiconductor Schottky junction

Maxim Trushin
Centre for Advanced 2D Materials, National University of Singapore, 6 Science Drive 2, Singapore 117546

(Received 28 February 2018; accepted 12 April 2018; published online 25 April 2018)

The standard theory of thermionic emission developed for three-dimensional semiconductors does not apply to two-dimensional materials even for making qualitative predictions because of the vanishing out-of-plane quasiparticle velocity. This study reveals the fundamental origin of the out-of-plane charge carrier motion in a two-dimensional conductor due to the finite quasiparticle lifetime and huge uncertainty of the out-of-plane momentum. The theory is applied to a Schottky junction between graphene and a bulk semiconductor to derive a thermionic constant, which, in contrast to the conventional Richardson constant, is determined by the Schottky barrier height and Fermi level in graphene. *Published by AIP Publishing*. https://doi.org/10.1063/1.5027271

Microelectronic devices employing thermionic emission over the Schottky barrier between graphene and silicon[1–26] or another bulk semiconductor[1,2,27–32] have experienced a boom over the last few years, see Refs. 33–35 for the most recent reviews. Graphene-semiconductor Schottky junctions possess rectification properties[1,3–5,13,15,27–29,31] and can be used in photodetection[7–13,18–26,36] as well as in solar energy harvesting.[6,14] The Schottky barrier height, Φ_B, is determined by the difference between the work function of graphene and semiconductor affinity, see Fig. 1. Since the work function depends on the Fermi energy E_F (which is tunable in graphene by an external electric field), the barrier height depends on the bias voltage across the junction.[1,33] The thermionic current density through an ideal Schottky junction (i.e. no thermionic field emission, no series resistance, etc.) then reads[33,37]

$$j = j_0\left(e^{\frac{eV}{k_BT}} - 1\right), \tag{1}$$

where e is the elementary charge, k_B is the Boltzmann constant, V is the bias voltage, and T is the electron temperature. The reverse saturation current density, j_0, flows across the junction when a reverse bias voltage ($V < 0$) pushes the electrons from graphene over the Schottky barrier to the semiconductor side. The goal of this letter is to derive j_0 for a two-dimensional (2D) conductor and apply the obtained formula to the graphene-semiconductor junction shown in Fig. 1.

The theoretical difficulties in modeling thermionic emission from 2D materials have been recognized only recently.[2,4,38–44] Indeed, thermionic emission from a surface of a bulk material is due to (i) electron energy high enough to overcome the work function difference at the interface and (ii) non-zero electron velocity normal to the surface. Electron kinetic energy can be controlled equally well in three-dimensional (3D) as well as in 2D conductors by heating. However, electrons in a 2D conductor (like graphene, which consists of only a surface) do not possess an out-of-plane velocity and it is not clear where it should come from. In an attempt to circumvent this issue, Sinha and Lee have introduced an empirical carrier injection rate[4] (see also Refs. 38 and 44) whereas Liang and Ang[39] have assumed a certain energy dispersion for the out-of-plane carrier motion, see also Refs. 2, 40–43 for further elaboration of their approach. Despite their reasonable agreement with experiments,[2,4] the models introduced until now are not self-contained (i.e. they require an external parameter) and, most importantly, do not explain *why* the 2D carriers do actually move out of plane. Hence, the fundamental origin of the out-of-plane carrier velocity in thermionic emission from a 2D conductor is still unclear. Here, I fill this gap using the concept of a hot electron liquid confined in a 2D plane.

The quasiparticle concept is a cornerstone of the electron liquid theory at finite temperatures: Any given charge carrier does not stay in its state forever but may fall down or be excited to any other empty state provided by energy and momentum conservation. Hence, a quasiparticle state with energy near the Fermi level E_F possesses a finite lifetime given by[45] $\tau_{E_F} \sim \hbar E_F/(k_BT)^2$. This estimation is valid for any normal metal, no matter 2D or 3D,[46] as long as $E_F \gg k_BT$. In intrinsic graphene, however, the Fermi surface shrinks to a single point that results in a 2D Dirac liquid[46] with the quasiparticle lifetime $\tau_0 \sim \hbar/(k_BT)$. This lifetime

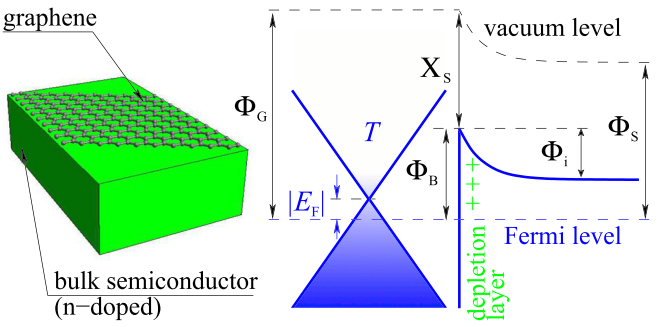

FIG. 1. Graphene placed on top of a bulk n-doped semiconductor forms a Schottky junction. Here, Φ_G and Φ_S are the work functions of graphene and the semiconductor, respectively, $\Phi_G > \Phi_S$ for Schottky contacts, E_F is the Fermi energy level counted from the band crossing point in graphene ($E_F < 0$ in the configuration shown), T is the carrier temperature in graphene, X_S is the semiconductor affinity (independent of E_F), Φ_i is the built-in potential created by the immobile ionized donors (green crosses), and Φ_B is the Schottky barrier. The in-plane band structure is shown for carriers in graphene. For the bulk semiconductor, only the bottom of the conduction band is shown. The gradient filling shows the relative population of the bands due to finite temperature.

can be seen as a mean time between the quasiparticle creation and annihilation events thanks to a time-independent perturbation. Within this lifetime, τ, a quasiparticle may acquire a certain perturbation-independent energy difference ΔE suggested by the energy uncertainty relation $\Delta E = \hbar/\tau$. In contrast to ΔE, the out-of-plane momentum uncertainty $\Delta p_z \sim \hbar/\Delta z$ is a constant determined solely by the single atomic layer thickness Δz being of the order of 1 Å. Thanks to the finite Δp_z, a quasiparticle may acquire a finite out-of-plane velocity, $v_z = \Delta E/\Delta p_z$.[47] Assuming that the initial out-of-plane velocity is zero, one can write the following formula for the velocity v_z that a quasiparticle acquires within the quasiparticle lifetime τ:

$$v_z \Delta p_z \sim \hbar/\tau. \tag{2}$$

Equation (2) shows that the finite quasiparticle momentum uncertainty and lifetime are *both* necessary to correctly evaluate the out-of-plane velocity. As long as the quasiparticle momentum may fluctuate within the uncertainty interval Δp_z, the quasiparticle acquires the finite velocity v_z. The shorter the quasiparticle lifetime is the higher velocity the quasiparticle has. The out-of-plane velocity vanishes only at absolute zero temperature when $\tau \to \infty$. In the case of zero momentum uncertainty (bulk limit, $\Delta z \to \infty$), the out-of-plane velocity becomes disentangled from the energy uncertainty[47] and is given by the standard relation $v_z = p_z/m^*$ in terms of an effective mass m^*.

The major merit of Eq. (2) is to evaluate the out-of-plane quasiparticle velocity without the ill-defined quasiparticle injection time or out-of-plane effective mass. For quasiparticles in intrinsic graphene with $\tau = \tau_0$ and T of a few hundreds of kelvins, one can estimate $v_z \sim 10^6$ cm/s, i.e. it is two orders of magnitude lower than the in-plane Fermi velocity $v_F \sim 10^8$ cm/s. If graphene is doped (say, $E_F \sim 0.2$ eV), then $\tau = \tau_{EF}$ and the out-of-plane velocity is even lower, $v_z \sim 10^5$ cm/s.

Let us apply Eq. (2) to an atomically thin conductor that forms a Schottky junction with a bulk semiconductor. The reverse saturation current density in Eq. (1) can be calculated by integrating the out-of-plane velocity over the quasiparticle states with energies above the barrier as

$$j_0 \sim e g_{sv} \frac{v_z \Delta p_z}{2\pi\hbar} \int \frac{dp_y}{2\pi\hbar} \int \frac{dp_x}{2\pi\hbar} f^{(0)}_{E_{p_x p_y}}, \tag{3}$$

where g_{sv} is the spin/valley degeneracy, $f^{(0)}_{E_{p_x p_y}}$ is the hot Fermi-Dirac distribution, $p_{x,y}$ (p_z) are the in-plane (out-of-plane) components of the quasiparticle momentum, and, in contrast to the conventional approach,[48] the integral over p_z has been substituted by its uncertainty Δp_z. Equation (3) is approximate and becomes applicable once the characteristic electron momentum (e.g. the Fermi momentum in metals) gets comparable with its uncertainty, or, in other words, the quasiparticle de Broglie wavelength becomes comparable with the conductor thickness. The integral over p_z should be retained otherwise.

For a graphene-semiconductor Schottky junction shown in Fig. 1, we have $f^{(0)}_{E_{p_x p_y}} \sim \exp\left(\frac{E_F - E_{p_x p_y}}{k_B T}\right)$ at $k_B T \ll \Phi_B$ with $E_{p_x p_y} = v_F \sqrt{p_x^2 + p_y^2}$ for electrons above the barrier, $g_{sv} = 4$, and Eq. (3) then reads

$$j_0 \sim \frac{e}{\tau} \int_{\Phi_B + E_F}^{\infty} \frac{dE E}{\pi^2 \hbar^2 v_F^2} e^{\frac{E_F - E}{k_B T}}, \quad k_B T \ll \Phi_B, \tag{4}$$

where $\Phi_B = \Phi_{B0} - E_F$ with Φ_{B0} being the Schottky barrier height at $E_F = 0$, see Fig. 1. In the case of intrinsic graphene ($|E_F| \ll k_B T$, $\tau = \tau_0$), we have

$$j_0 \sim A^*_{G0} T^2 e^{-\frac{\Phi_B}{k_B T}}, \quad |E_F| \ll k_B T. \tag{5}$$

Here, $A^*_{G0} = e(\Phi_{B0} + k_B T) k_B^2/(\pi^2 \hbar^3 v_F^2)$ is the thermionic constant for intrinsic graphene. Since $k_B T$ is much lower than Φ_{B0}, the former can be neglected in A^*_{G0}, and the current density obeys the Richardson-Dushman law,[49] where the reverse saturation current is given by $j_0 = A^* T^2 \exp[-\Phi_B/(k_B T)]$ with $A^* = e m^* k_B^2/(2\pi^2 \hbar^3)$ being the Richardson constant.[48,49] In contrast to the conventional Richardson constant, A^*_{G0} strongly depends on the barrier height Φ_{B0}. For Φ_{B0} of the order of 0.1 eV (see Table 1 in Ref. 33), we estimate A^*_{G0} to be about 10 A cm^2 K^2 that is comparable with the Richardson constant $A^* = 120\ (m^*/m_0)$ A cm^{-2} K^{-2}, where the effective-to-free electron mass ratio m^*/m_0 is of the order of 0.1 for typical bulk metal-semiconductor junctions.[50] One could define an out-of-plane effective mass for carriers in graphene as $m^* v_F^2/2 = \Phi_B$ and utilize the standard formula for A^*. The Schottky barrier height plays therefore a role of the effective electron mass in the conventional theory of thermionic emission. This makes sense because both the Schottky barrier and inertial mass resist the out-of-plane particle acceleration.

In the case of doped graphene ($|E_F| \gg k_B T$, $\tau = \tau_{E_F}$), Eq. (4) reads

$$j_0 \sim \frac{e(\Phi_{B0} + k_B T) k_B^3 T^3}{\pi^2 \hbar^3 v_F^2 |E_F|} e^{-\frac{\Phi_B}{k_B T}}, \quad k_B T \ll |E_F|, \tag{6}$$

where E_F can be positive or negative depending on graphene doping, and T^3-dependence indicates that the Richardson-Dushman law becomes invalid. Nevertheless, one can formally define the temperature dependent thermionic constant as $A^*_G = A^*_{G0} \frac{k_B T}{|E_F|}$. Hence, the thermionic constant is further reduced as compared with the intrinsic value A^*_{G0} and could therefore partly explain why its actual value measured in graphene-silicon junctions is smaller than expected.[4] The temperature dependence of j_0 given by Eq. (6) at $\Phi_{B0} \gg k_B T$ is similar to what has been predicted by Liang and Ang[39] but, in contrast to their model, A^*_G is governed by Φ_{B0} and E_F, not just by the fundamental constants and Fermi velocity in graphene.

The thermionic constant turns out to be strongly dependent on the Fermi energy and offers an interesting opportunity to test the model predictions in real devices. The constant increases while the Fermi level approaches the band crossing point in graphene until it reaches the intrinsic value A^*_{G0} at $|E_F| \ll k_B T$. The trend is schematically shown in Fig. 2 at $\Phi_{B0} \sim 0.5$ eV. The saturation current, however, does not follow this trend since the inverse proportion to E_F is by far compensated for by the exponential dependence on E_F via Φ_B. Anyway, the thermionic constant can easily be identified by plotting $j_0(E_F)$ on a logarithmic scale and subtracting the trivial Φ_B/T term.[50]

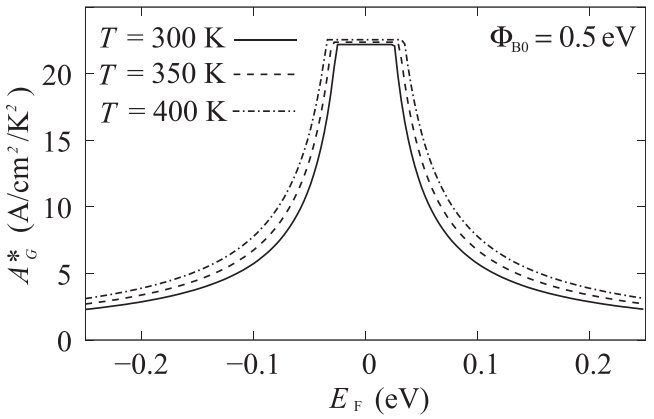

FIG. 2. Schematic plot of the thermionic constant A_G^* vs. the Fermi energy E_F, as defined below Eq. (6). Since A_G^* diverges at $E_F = 0$, it is substituted by the intrinsic value A_{G0}^* once A_G^* becomes larger than A_{G0}^*. The intrinsic value is defined below Eq. (5).

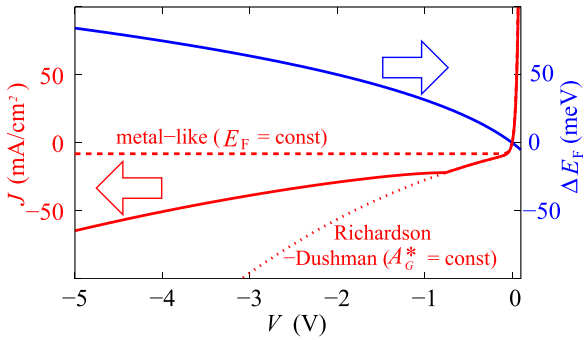

FIG. 3. Typical current-voltage characteristics (solid red line) plotted for an intrinsic graphene/n-type semiconductor Schottky junction ($\Phi_{B0} \sim 0.5$ eV, $T \sim 300$ K) by means of Eq. (1) with j_0 given by either Eqs. (5) or (6), depending on E_F. The dotted line corresponds to the conventional Richardson-Dushman model with the thermionic constant $A_G^* = A_{G0}^*$ assumed to be independent of the Fermi energy E_F. The dashed line describes the metal-like model when the Fermi energy does not depend on the bias voltage V so that the saturation current, j_0, remains constant. The blue solid line is the (quasi-)Fermi energy shift in graphene due to the carrier density induced by the bias voltage. The parameters are discussed in the main text.

In contrast to conventional metal-semiconductor diodes, graphene-semiconductor junctions demonstrate a bias-driven increase in the reverse saturation current.[1,33] To be specific, let us consider the current-voltage characteristics of a junction between graphene and an n-doped semiconductor assuming that the Fermi level intercepts the band crossing point in graphene at zero bias (see Fig. 17 in Ref. 33). A bias voltage redistributes the positive and negative charge across the junction, resulting in two different (quasi)-Fermi levels for carriers on the graphene and semiconductor sides. The forward bias ($V > 0$) lowers the positive charge of the depletion layer in the semiconductor, hence reducing the built-in potential Φ_i at the interface as well as the Fermi energy in graphene. In contrast, the reverse bias ($V < 0$) extends the depletion layer to the semiconductor side increasing the built-in potential. At the same time, the Fermi level increases in graphene because of the higher charge density induced there to mirror the excessive immobile donor charge of the depletion layer. The induced charge density can be calculated using the Schottky-Mott relationship as[33]

$$-e\Delta n_{\text{ind}} = \sqrt{2\epsilon_S N_D(\Phi_i - eV - k_B T)} - \sqrt{2\epsilon_S N_D(\Phi_i - k_B T)}, \tag{7}$$

where $\epsilon_S \sim 10$ is the relative permittivity of a typical semiconductor, $N_D \sim 10^{16}\,\text{cm}^{-3}$ is the donor concentration in the depletion layer, and $\Phi_i \sim 0.6$ eV is the built-in potential. The typical parameter values are taken from Ref. 1 where various graphene/n-type semiconductor junctions have been studied. The Fermi energy difference due to the reverse bias can be written for graphene as $\Delta E_F = \hbar v_F \sqrt{-\pi \Delta n_{\text{ind}}}$, where the four-fold degeneracy has been taken into account in the relation between the Fermi wave vector and the carrier concentration. The blue line in Fig. 3 demonstrates that the reverse bias results in a transfer of negative charge to graphene large enough to increase ΔE_F by tens of meV at the voltages of a few volts, in accordance with the measurements of Ref. 1. The upward shift of E_F in graphene causes a reduction of the barrier height Φ_B facilitating electron transport across the junction and preventing the reverse current from saturating. If graphene behaved like a regular metal with a very high density of states, then the Fermi energy would not change much under the bias voltage resulting in a nearly constant j_0 and perfect saturation of the reverse current (see the red dashed line in Fig. 3). Retaining the exponential dependence j_0 on E_F but neglecting the substantial decrease in the thermionic constant at higher $|E_F|$ allows us to qualitatively reproduce the lack of the reverse current saturation observed in real graphene-semiconductor junctions[1] (see the red dotted line in Fig. 3). In fact, the inverse proportion of j_0 to E_F read out from Eq. (6) partly compensates for this exponential trend. The result is that the true reverse current values shown by the red solid line in Fig. 3 lie between the curves given by Eq. (5) with $E_F = 0$ assumed to be independent of V (the metal-like model, dashed curve) and by the same equation with $E_F = \Delta E_F(V)$ (the Richardson-Dushman law, dotted curve).

The experimental verification of the model proposed is obviously of the utmost importance for graphene-based device applications as the reverse saturation current is one of the most essential parameters to characterize a Schottky diode. The previous transport measurements[1] have employed samples fabricated from graphene grown on copper by chemical vapor deposition and subsequently transferred onto a semiconductor. Graphene has been found to be p-doped with the Fermi energy $|E_F| \gtrsim 200$ meV being much higher than ΔE_F provided by the bias voltage (see Fig. 3). It was therefore impossible to observe the qualitative change of the saturation current behavior due to the crossover between intrinsic ($|E_F| \ll k_B T$) and highly doped ($k_B T \ll |E_F|$) regimes. Moreover, the reverse current seen in Fig. 3 is much higher than the measured one[1] because the Schottky barrier is almost 0.3 eV lower in our case of intrinsic graphene. To see the effects predicted above, one needs much cleaner samples with $|E_F| \lesssim 25$ meV at zero bias. Nevertheless, the T^3-dependence in the saturation current for doped graphene predicted by Eq. (6) can be verified by using existing experimental data[2] for graphene contacts with Si, MoS_2, GaAs, and GaN. Indeed, the measured current density plotted as $\ln(j_0/T^3)$ vs. $1/T$ demonstrates a linear dependence for any of the four bulk semiconductors considered. This is a clear indication of consistency between the theory and experimental data available at the moment.

Besides possible applications, the experiments with nearly intrinsic graphene might shed some light on the fundamental properties of a Dirac liquid confined in a 2D plane (see Ref. 46 for review). Indeed, the most important ingredient of the model introduced above is the quasiparticle lifetime which is $\tau_0 \sim \hbar/(k_B T)$ in the intrinsic limit. Interestingly, an emission rate equal to $k_B T/\hbar$ has been obtained in Ref. 44 by fitting the thermionic constant for a 2D electron gas with the Richardson-Dushman law. Here, we associate the emission rate with the inverted quasiparticle lifetime, which makes a lot of sense as τ_0 can be seen as the average time needed to repopulate a given state above the barrier after emission. Once the Fermi energy is shifted away from the band crossing point in graphene, the quasiparticle lifetime decreases rapidly and, as a consequence, the thermionic constant is reduced. Since the Fermi energy depends on the bias voltage, this effect should be seen in the current-voltage measurements. Alternatively, the Fermi energy of graphene can be varied through appropriate gating.[3,51]

The intimate relation between the quasiparticle emission rate and lifetime is among the main findings of this work. The model explains, above all, why the quasiparticles tightly confined in a 2D plane still possess an out-of-plane velocity. The thermionic emission mechanism in graphene-semiconductor junctions strongly differs from its bulk version. The Richardson constant employed in the conventional model is substituted by the thermionic constant A_G^* that depends on the Fermi energy that is in turn tunable by an external electric field normal to the graphene plane.

Graphene-semiconductor junctions should demonstrate efficient photocarrier injection with excitation energy below the semiconductor bandgap. The photocarriers excited in graphene are thermalized rapidly[52,53] creating a high-energy distribution tail above the Schottky barrier, hence providing excess energy necessary for thermionic emission across the interface. In contrast to the conventional heterojunctions,[54,55] the out-of-plane momentum conservation is relaxed by the momentum uncertainty $\Delta p_z \sim \hbar/\Delta z$, which, thanks to the small layer thickness Δz, is of the order of the first Brillouin zone size. The interface disorder thereby does not much hamper the out-of-plane carrier transport between graphene and the semiconductor. The injection rate is governed by the quasiparticle lifetime rather than the interface disorder. Hence, the carriers do not behave like point-like particles along the z-direction until they turn out to be on the semiconductor side with a well-defined momentum. This peculiarity should be taken into account when designing optoelectronic devices based on 2D materials.

I would like to thank Ilya Goykhman and Andrea Ferrari for turning my attention to the problem of thermionic emission from graphene. Multiple discussions with Shi-Jun Liang are also acknowledged. This work was supported by the Director's Senior Research Fellowship from the Centre for Advanced 2D Materials at the National University of Singapore (NRF Medium Sized Centre Programme R-723-000-001-281).

[1]S. Tongay, M. Lemaitre, X. Miao, B. Gila, B. R. Appleton, and A. F. Hebard, Phys. Rev. X **2**, 011002 (2012).
[2]S.-J. Liang, W. Hu, A. Di Bartolomeo, S. Adam, and L. K. Ang, in *2016 IEEE International Electron Devices Meeting (IEDM)* (IEEE, 2016), p. 14.
[3]H. Yang, J. Heo, S. Park, H. J. Song, D. H. Seo, K.-E. Byun, P. Kim, I. Yoo, H.-J. Chung, and K. Kim, Science **336**, 1140 (2012).
[4]D. Sinha and J. U. Lee, Nano Lett. **14**, 4660 (2014).
[5]C.-C. Chen, M. Aykol, C.-C. Chang, A. Levi, and S. B. Cronin, Nano Lett. **11**, 1863 (2011).
[6]Y. Song, X. Li, C. Mackin, X. Zhang, W. Fang, T. Palacios, H. Zhu, and J. Kong, Nano Lett. **15**, 2104 (2015).
[7]I. Goykhman, U. Sassi, B. Desiatov, N. Mazurski, S. Milana, D. de Fazio, A. Eiden, J. Khurgin, J. Shappir, U. Levy *et al.*, Nano Lett. **16**, 3005 (2016).
[8]F. Liu and S. Kar, ACS Nano **8**, 10270 (2014).
[9]X. Li, M. Zhu, M. Du, Z. Lv, L. Zhang, Y. Li, Y. Yang, T. Yang, X. Li, K. Wang *et al.*, Small **12**, 595 (2016).
[10]M. Zhu, L. Zhang, X. Li, Y. He, X. Li, F. Guo, X. Zang, K. Wang, D. Xie, X. Li *et al.*, J. Mater. Chem. A **3**, 8133 (2015).
[11]X. An, F. Liu, Y. J. Jung, and S. Kar, Nano Lett. **13**, 909 (2013).
[12]Y. An, A. Behnam, E. Pop, and A. Ural, Appl. Phys. Lett. **102**, 013110 (2013).
[13]Y. An, A. Behnam, E. Pop, G. Bosman, and A. Ural, J. Appl. Phys. **118**, 114307 (2015).
[14]T. Jiao, D. Wei, X. Song, T. Sun, J. Yang, L. Yu, Y. Feng, W. Sun, W. Wei, H. Shi *et al.*, RSC Adv. **6**, 10175 (2016).
[15]Y.-J. Lin, Superlattices Microstruct. **88**, 645 (2015).
[16]C. Yim, N. McEvoy, and G. S. Duesberg, Appl. Phys. Lett. **103**, 193106 (2013).
[17]S. Parui, R. Ruiter, P. Zomer, M. Wojtaszek, B. Van Wees, and T. Banerjee, J. Appl. Phys. **116**, 244505 (2014).
[18]X. Wang, Z. Cheng, K. Xu, H. K. Tsang, and J.-B. Xu, Nat. Photonics **7**, 888 (2013).
[19]M. Amirmazlaghani, F. Raissi, O. Habibpour, J. Vukusic, and J. Stake, IEEE J. Quantum Electron. **49**, 589 (2013).
[20]P. Lv, X. Zhang, X. Zhang, W. Deng, and J. Jie, IEEE Electron Device Lett. **34**, 1337 (2013).
[21]Z. Chen, Z. Cheng, J. Wang, X. Wan, C. Shu, H. K. Tsang, H. P. Ho, and J.-B. Xu, Adv. Opt. Mater. **3**, 1207 (2015).
[22]S. Riazimehr, A. Bablich, D. Schneider, S. Kataria, V. Passi, C. Yim, G. S. Duesberg, and M. C. Lemme, Solid-State Electron. **115**, 207 (2016).
[23]S. Riazimehr, S. Kataria, R. Bornemann, P. Haring Bolívar, F. J. G. Ruiz, O. Engström, A. Godoy, and M. C. Lemme, ACS Photonics **4**, 1506 (2017).
[24]J. Shen, X. Liu, X. Song, X. Li, J. Wang, Q. Zhou, S. Luo, W. Feng, X. Wei, S. Lu *et al.*, Nanoscale **9**, 6020 (2017).
[25]A. Di Bartolomeo, G. Luongo, F. Giubileo, N. Funicello, G. Niu, T. Schroeder, M. Lisker, and G. Lupina, 2D Mater. **4**, 025075 (2017).
[26]H. Selvi, N. Unsuree, E. Whittaker, M. P. Halsall, E. W. Hill, A. Thomas, P. Parkinson, and T. J. Echtermeyer, Nanoscale **10**, 3399 (2018).
[27]W. Kim, C. Li, F. A. Chaves, D. Jiménez, R. D. Rodriguez, J. Susoma, M. A. Fenner, H. Lipsanen, and J. Riikonen, Adv. Mater. **28**, 1845 (2016).
[28]D. Tomer, S. Rajput, L. Hudy, C. Li, and L. Li, Appl. Phys. Lett. **106**, 173510 (2015).
[29]A. Kumar, R. Kashid, A. Ghosh, V. Kumar, and R. Singh, ACS Appl. Mater. Interfaces **8**, 8213 (2016).
[30]E. M. Mills, B. K. Min, S. K. Kim, S. J. Kim, M.-A. Kang, W. Song, S. Myung, J. Lim, K.-S. An, J. Jung *et al.*, ACS Appl. Mater. Interfaces **7**, 18300 (2015).
[31]Z. Khurelbaatar, Y.-H. Kil, K.-H. Shim, H. Cho, M.-J. Kim, Y.-T. Kim, and C.-J. Choi, J. Semicond. Technol. Sci. **15**, 7 (2015).
[32]N. Poudel, S.-J. Liang, D. Choi, B. Hou, L. Shen, H. Shi, L. K. Ang, L. Shi, and S. Cronin, Sci. Rep. **7**, 14148 (2017).
[33]A. Di Bartolomeo, Phys. Rep. **606**, 1 (2016).
[34]D. Xu, X. Yu, L. Yang, and D. Yang, Superlattices Microstruct. **99**, 3 (2016).
[35]Y. Xu, C. Cheng, S. Du, J. Yang, B. Yu, J. Luo, W. Yin, E. Li, S. Dong, P. Ye *et al.*, ACS Nano **10**, 4895 (2016).
[36]A. Di Bartolomeo, F. Giubileo, G. Luongo, L. Iemmo, N. Martucciello, G. Niu, M. Fraschke, O. Skibitzki, T. Schroeder, and G. Lupina, 2D Mater. **4**, 015024 (2016).
[37]C. Crowell and S. Sze, Solid-State Electron. **9**, 1035 (1966).
[38]A. Varonides, Phys. Status Solidi (c) **13**, 1040 (2016).
[39]S.-J. Liang and L. K. Ang, Phys. Rev. Appl. **3**, 014002 (2015).
[40]Y. Ang and L. Ang, Phys. Rev. Appl. **6**, 034013 (2016).
[41]Y. S. Ang, M. Zubair, K. Ooi, and L. Ang, Phys. Rev. Appl. (submitted); e-print arXiv:1711.05898 (2017).
[42]M. Upadhyay Kahaly, S. Misra, and S. Mishra, J. Appl. Phys. **121**, 205110 (2017).

[43]S. Misra, M. Upadhyay Kahaly, and S. Mishra, J. Appl. Phys. **121**, 065102 (2017).
[44]X. Wei, Q. Chen, and L. Peng, AIP Adv. **3**, 042130 (2013).
[45]A. A. Abrikosov, *Fundamentals of the Theory of Metals* (Elsevier Science Pub. Co. Inc., New York, NY, 1988).
[46]A. Lucas and K. C. Fong, J. Phys.: Condens. Matter **30**, 053001 (2018).
[47]L. D. Landau and E. M. Lifshitz, *Quantum Mechanics: Non-Relativistic Theory* (Elsevier, 2013), Vol. 3.
[48]C. Crowell, Solid-State Electron. **8**, 395 (1965).
[49]S. Dushman, Rev. Mod. Phys. **2**, 381 (1930).
[50]M. Missous and E. Rhoderick, J. Appl. Phys. **69**, 7142 (1991).
[51]C.-C. Chen, C.-C. Chang, Z. Li, A. Levi, and S. B. Cronin, Appl. Phys. Lett. **101**, 223113 (2012).
[52]E. Malic, T. Winzer, and A. Knorr, Appl. Phys. Lett. **101**, 213110 (2012).
[53]D. Brida, A. Tomadin, C. Manzoni, Y. J. Kim, A. Lombardo, S. Milana, R. R. Nair, K. Novoselov, A. C. Ferrari, G. Cerullo *et al*., Nat. Commun. **4**, 1987 (2013).
[54]C. Wu and E. Yang, Solid-State Electron. **22**, 241 (1979).
[55]R. Kim, C. Jeong, and M. S. Lundstrom, J. Appl. Phys. **107**, 054502 (2010).